An Integrated Navigation Method for UAV Autonomous Landing Based on Inertial and Vision Sensors

Kejun Shang(✉), Xixi Li, Chongliang Liu, Li Ming, and Guangfeng Hu

Beijing Institute of Automation Equipment, Beijing 100074, China
kjshang@163.com, bridge968@sina.com

Abstract. In the process of autonomous landing of unmanned aerial vehicles (UAV), the vision sensor is restricted by the field of view and UAV maneuvering process, which may make the acquired relative position/attitude parameters unstable or even odd (not unique), and there is a 'blind area' of vision measurement in the UAV rollout stage, which loses the navigation ability and seriously affects the safety of landing. In this paper, an autonomous landing navigation method based on inertial/visual sensor information fusion is proposed. When the UAV is far away from the airport and the runway imaging is complete, landing navigation parameters are determined by vision sensor based on the object image conjugate relationship of the runway sideline, and fuses with the inertial information to improve the measure performance. When the UAV is close to the airport and the runway imaging is incomplete, the measurement information of the vision sensor appears singular. The estimation of the landing navigation parameters is realized by inertial information in the aid of vision. When the UAV rollouts, the vision sensor enters the 'blind area', judges the UAV's motion state through the imaging features of two adjacent frames, and suppresses the inertial sensor error by using the UAV's motion state constraint, so as to achieve the high-precision maintenance of landing navigation parameters. The flight test shows that the lateral relative position error is less than 10m when the inertial with low accuracy and visual sensor are used, which can meet the requirement of UAV landing safely.

Keywords: Autonomous landing navigation · Deep learning semantic segmentation · Inertial/Vision data fusion

1 Introduction

Autonomous landing of UAV refers to the positioning, navigation and control of UAV relying its own flight control system and various navigation equipment. The aim is to guide the UAV to land on the runway independently and safely. It is the premise of safe recovery and reuse of UAV in complex environment. Research data indicate that the number of faults in landing process accounts for more than 80% of the total faults in UAV mission profile. For the fixed wing UAV with fast flight speed and no hovering function, the landing process is more complex and the risk is higher. Accurate measurement

L. Fang et al. (Eds.): CICAI 2022, LNAI 13605, pp. 182–193, 2022.
https://doi.org/10.1007/978-3-031-20500-2_15

of relative position/attitude between UAV and runway is the key to safe landing and navigation. At present, the main methods of radio positioning and satellite difference real-time positioning are lack of information integrity, anti-interference ability and data update frequency.

In recent years, based on the visual navigation technology, people take the runway plane as the cooperative target, determine the relative geometric relationship between the UAV and the airport runway through the visual sensor during landing, and then obtain the relative position/attitude between them. This method has a great advantage in the measurement accuracy, and has been gradually verified by the engineering application, causing extensive research internationally [1, 2]. Wand and Zhou use AprilTag markers as tracking targets for the landing navigation of rotor wing UAV [3, 4]. However, fixed wing UAVs landing on airport runways cannot use additional tracking targets except runway. Wang and Zhang propose navigation methods based on runway detection and visual-inertial fusion, when the runway features imaging integrated [5, 6]. However, the acquired relative position/attitude may be unstable or even singular due to the constraints of visual sensor's field of view, installation position, UAV's maneuver mode and flight environment. When the UAV approaches the starting line of the runway and enters the rollout stage, the runway imaging is incomplete, there is not enough feature lines for navigation due to the starting line losing and relative narrow field of view (the camera is about 1.5 m above the ground). Then the UAV enter into the 'blind area' of visual measurement, which brings a huge potential safety hazard to the landing [7–9].

To solve the above problems, this paper proposes an autonomous landing navigation method based on the information fusion of inertial/visual sensors. When the UAV is far away from the airport and the runway image is complete, the landing navigation parameters of UAV are determined based on the object image conjugate relationship of the runway characteristic line of visual sensors [10, 11]. When the UAV is close to the airport and the runway imaging is incomplete, the measurement information of the visual sensor appears singular, and the UAV landing and navigation parameters are estimated by the information of the inertial sensor assisted by the visual information. In the stage of the UAV's touchdown and rollout, the visual sensor enters the 'blind area', and judges the UAV's motion state by the imaging features of two adjacent frames in order to improve the measurement accuracy and reliability of landing navigation information.

2 Landing Process Analysis and Scheme Design

Taking a typical landing flight profile of a fixed wing UAV as an example (as shown in Fig. 1), the landing process is divided into 4 areas:

Area A: $x_l < K_1$. As shown in Fig. 2(a), the runway imaging is represented as a 'point target', so the relative position/attitude information cannot be calculated in the visual sensor coordinate system.

Area B: $K_1 \leq x_l < K_2$. As shown in Fig. 2(b), high-precision relative position/attitude measurement information can be obtained in the visual sensor coordinate system and then fuses with inertial navigation information to improve the performance.

Area C: $K_2 \leq x_l < K_3$. As shown in Fig. 2(c), it is not sufficient for visual measurement. The relative position/attitude can be acquired with the aid of inertial sensor.

Area D: $K_3 \leq x_l < K_4$. As shown in Fig. 2(d), the runway center line is clearly visible, which can be used to judge the motion state of UAV and assist to realize the inertial navigation error suppression based on motion constraints.

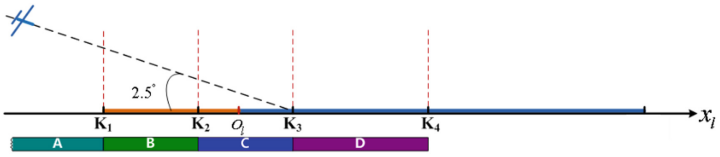

Fig. 1. The typical landing process of UAV

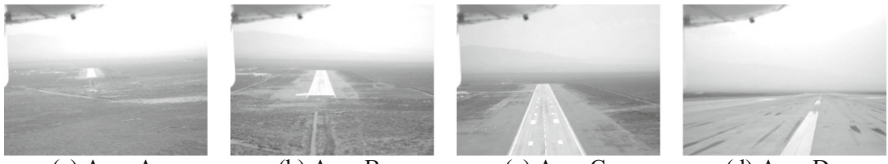

(a) Area A (b) Area B (c) Area C (d) Area D

Fig. 2. Visual features during UAV's typical landing process

3 Intelligent Identification of Airport Runway Based on Deep Learning Semantic Segmentation

3.1 Runway Segmentation Network Design

The runway area is defined as the area between the left line, the right line, the start line and the end line of the runway, as shown in the quadrilateral area with A, B, E, F as the vertices in Fig. 3.

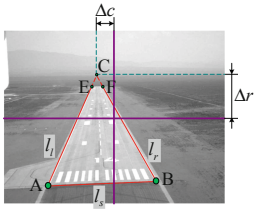

Fig. 3. Definition of runway area

When designing the segmentation network, the segmentation accuracy and multi-scale feature extraction ability of the network should also be improved while focusing on the real-time calculation.

As shown in Fig. 4, the runway segmentation network (named RunwayNet [12]) adopts an encoder-decoder structure, and the encoder consists of a backbone network and a self-attention module. The Network Backbone is a lightweight ShuffleNet V2 modified by Atrous Convolution or Dilated Convolutions, which gradually extracts abstract semantic features from the input image, and finally outputs feature map; the self-attention module performs feature transformation on the feature map output by the backbone network through two sub-modules of positional attention and channel attention to capture the similarity of feature map spatial dimension and channel dimension information to improve the receptive field and feature extraction ability of the network. The decoder module realizes the fusion of rich details and spatial location information in the shallow layer of the network with the rough and abstract semantic segmentation information in the top layer through skip connections and bilinear interpolation upsampling. Finally, use convolution to map the output feature map of the decoder into two channels (number of classification categories), and after upsampling 8 times, take the maximum value (ArgMax) in the channel dimension to obtain the final segmentation result.

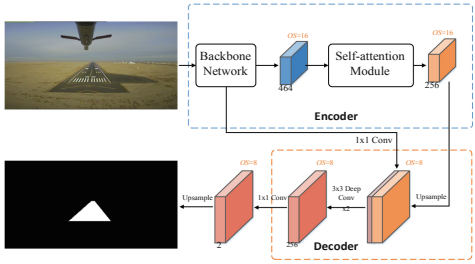

Fig. 4. RunwayNet network architecture

3.2 Runway Edge Feature Extraction

First, contour detection is performed, and the landing stage is judged according to the proportion of the runway contour. Then the spatial characteristics of the runway area are calculated, and the barycentric coordinates of the runway contour and the perimeter of the contour are calculated according to the space moment. Then the candidate line segment is fitted and run to the sideline. In order to further eliminate the wrongly classified line segments entering the runway sideline, outliers are eliminated by comparing with the reference line segments in each category. Finally, first-order polynomial fitting is performed on each type of line segment group to obtain the coordinates of the corresponding straight line equation, and minimize the squared error through iteration to get the optimal solution of the straight line equation.

4 Modeling of Visual Relative Position/Attitude Measurement Based on the Characteristics of Runway Boundary

The edge line of the airport runway mainly includes the starting line l_s, left line l_l and right line l_r. In the imaging of the visual sensor, these three lines can form a triangle

[13, 14], as shown in Fig. 3. The model based on this inherent feature can uniquely determine the relative position/attitude between the visual sensor and the runway under the condition of accurately calibrating the geographic coordinates of four points A, B, E, F and the focal length of the visual sensor [15–17].

4.1 Coordinate System and Parameters Definition

The coordinate systems involved in this paper include earth coordinate system (*e* system), geographical coordinate system (*t* system), UAV coordinate system (*m* system), world coordinate system (*w* system), runway coordinate system (*l* system), visual sensor coordinate system (*c* system), image coordinate system (*i* system) and inertial sensor coordinate system (*b* system) [18, 19]. The relationship between *w* system and *c* system is shown in Fig. 5.

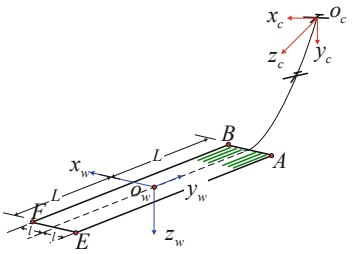

Fig. 5. The relationship between world and visual sensor coordinate system

Set the half-length and half-width of the runway as L and l, and the resolution of the visual sensor as m × n (rows × columns, unit: pixel). Define the relative attitude angles between the coordinate system of the visual sensor and the world coordinate system as the relative rolling angle γ_r, relative heading angle ψ_r and relative pitch angle θ_r, respectively. Then the rotation z_c axis ⇒ y_c axis ⇒ x_c axis with $-\gamma_r$, $-\psi_r$, $-\frac{\pi}{2} - \theta_r$ can match the *w* system. The conversion relationship between them is shown in Eq. (1) [20]

$$C_c^w = R_X\left(-\frac{\pi}{2} - \theta_r\right)R_Y(-\psi_r)R_Z(-\gamma_r) \tag{1}$$

4.2 Mathematical Modeling of Visual Relative Position/Attitude Measurement

Modeling of Object Image Conjugate Relation. Let a point P in the space in the image coordinate system be the homogeneous coordinate $P^c = [r \quad c \quad 1]^T$. The homogeneous coordinate in the world coordinate system is $P^w = \begin{bmatrix} x_w & y_w & z_w & 1 \end{bmatrix}^T$. The conjugate relationship between the object and the image is shown in Eq. (2) [21, 22]

$$P^c = s\tilde{K}\tilde{C}_w^c\tilde{T}'P^w \tag{2}$$

where $s = \frac{1}{z_c}$, and z_c is the z axis component of the space point P in the coordinate system c of the vision sensor. $\tilde{K}$ is the internal parameter array of the vision sensor. $\tilde{C}_w^c$ includes the relative attitude to be solved. $\tilde{T}'$ includes the relative position to be solved.

The process to get the relative position and attitude can be abstracted as a typical PNP problem [23, 24]. In this paper, the rectangle contour of runway composed of four vertices A, B, E and F, and the inherent features of two parallel sidelines and one starting line are used to calculate the relative position/attitude, which can avoid the problem that the measurement accuracy in the traditional solution method [5, 6] is seriously affected by the extraction error of feature point image.

Relative Attitude Solution. In the coordinate system of vision sensor, the left line l_l, the right line l_r And the starting line l_s are obtained by the feature extraction of runway. the equation can be described as

$$\begin{bmatrix} 1 & k_l & q_l \\ 1 & k_r & q_r \\ 1 & k_s & q_s \end{bmatrix} P^c = EP^c = \begin{bmatrix} 0 \\ 0 \\ 0 \end{bmatrix} \tag{3}$$

where k_i and $q_i (i = l, r, s)$ are the slope and intercept of three equations respectively.

Relative heading angle ψ_r will be reflected in the horizontal deviation Δc (unit: pixel) between and point C and the image center.

Relative rolling angle γ_r will be reflected in the slope of the starting line l_s.

Relative pitch angle θ_r will be reflected on the vertical deviation Δr (in pixels) between the C point and the image center point when imaging, so

$$\psi_r = -\arctan\left(\frac{d\,\Delta c}{f}\right), \gamma_r = \arctan(k_s), \theta_r = \arctan\left(\frac{d\,\Delta r}{f}\right) \tag{4}$$

Relative Position Solution. The equation can be sorted out as

$$\begin{bmatrix} 1 & \frac{a_3^l}{a_2^l} \\ 1 & \frac{a_3^r}{a_1^r} \end{bmatrix} \begin{bmatrix} t_x' \\ t_z' \end{bmatrix} = \begin{bmatrix} l \\ -l \end{bmatrix}, t_y' = -L - \frac{a_3^s}{a_2^s} t_z' \tag{5}$$

so the values of t_x' and t_z' and t_y' can be solved by Eq. (5).

However, when the airport runway image is incomplete or it enters the 'blind area' of visual measurement, the slope and intercept under the three characteristic edge image coordinate system of the runway cannot be obtained. The solution is singular, which brings security risks to UAV landing. The inertial/visual sensor information fusion technology presented in this paper aims to solve this problem.

5 Information Fusion Model of Inertial/Visual Sensor

The inertial/visual information fusion model used in relative position/attitude measurement during the whole landing process is shown in Fig. 6.

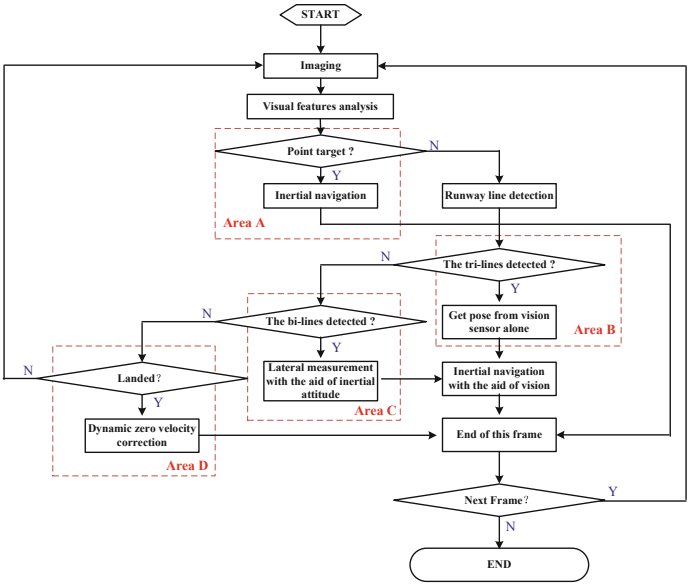

Fig. 6. Inertial/visual information fusion process

5.1 System State Equation

Select system status as

$$\boldsymbol{X} = \left[\boldsymbol{\delta v^t}\ \boldsymbol{\varphi^t}\ \boldsymbol{\delta P^t}\ \boldsymbol{\varepsilon}\ \nabla\ \boldsymbol{\delta\beta_\psi}\ \boldsymbol{\delta\beta_\theta}\ \boldsymbol{\delta\beta_\gamma}\ \boldsymbol{\delta\alpha_\theta}\ \boldsymbol{\delta\alpha_\psi} \right]^{\boldsymbol{T}} \tag{6}$$

where $\delta v^t = [\delta v_N^t\ \delta v_U^t\ \delta v_E^t]$, $\varphi^t = [\varphi_N^t\ \varphi_U^t\ \varphi_E^t]$, $\delta P^t = \left[\delta\phi\ \delta\lambda\ \delta h\right]$ are velocity, attitude and position errors calculated by inertial sensor; $\varepsilon = \left[\varepsilon_x\ \varepsilon_y\ \varepsilon_z\right]$ and $\nabla = [\nabla_x\ \nabla_y\ \nabla_z]$ are the bias stability parameters of three gyros and three accelerometers; $\delta\beta_\psi, \delta\beta_\theta, \delta\beta_\gamma$ are installation error angles between inertial and visual sensor in heading, pitch and roll direction; $\delta\alpha_\theta$ and $\delta\alpha_\psi$ represent installation error angles between inertial sensor and UAV body in pitch and heading direction respectively, which can be calculated by dead reckoning in area D.

It is considered that all installation error angles are constant, and the specific form of system error equation can be seen in relevant literature [25–30].

5.2 System Observation Equation

Position Error Equation. After compensating the lever arm error between the inertial sensor and the visual sensor, the position error of the inertial information can be calculated according to the following formula

$$\begin{bmatrix} \boldsymbol{\delta L} \\ \boldsymbol{\delta\lambda} \\ \boldsymbol{\delta h} \end{bmatrix} = \begin{bmatrix} \boldsymbol{L_{INS}} \\ \boldsymbol{\lambda_{INS}} \\ \boldsymbol{h_{INS}} \end{bmatrix} - \left(\begin{bmatrix} \frac{1}{(\boldsymbol{R_{Mo}}+\boldsymbol{h_o})} & 0 & 0 \\ 0 & \frac{1}{((\boldsymbol{R_{No}}+\boldsymbol{h_o})\boldsymbol{cos}(\boldsymbol{L_o}))} & 0 \\ 0 & 0 & 1 \end{bmatrix} \cdot \boldsymbol{C_w^t} \begin{bmatrix} \boldsymbol{t_x'} \\ \boldsymbol{t_y'} \\ \boldsymbol{t_z'} \end{bmatrix} + \begin{bmatrix} \boldsymbol{L_o} \\ \boldsymbol{\lambda_o} \\ \boldsymbol{h_o} \end{bmatrix} \right) \tag{7}$$

where, R_{Mo} and R_{No} are the curvature radii of the earth calculated by the coordinates of O_w points [20], $\left[L_{INS}\ \lambda_{INS}\ h_{INS}\right]^T$ are the latitude, longitude and height calculated by inertial sensors. $\left[L_o\ \lambda_o\ h_o\right]^T$ are the latitude, longitude and height of the central point of AB.

In area B, the relative position $\left[t_x^{'}\ t_y^{'}\ t_z^{'}\right]$ and relative attitude (included in C_w^t) measured by the visual sensor are directly used.

In area C, the attitude measurement information of vision sensor is singular. The installation error angle matrix C_c^b between inertial sensor and vision sensor, the matrix C_b^t and matrix C_t^w can be used to calculate the relative attitude matrix C_c^w. Then the relative position information $\left[t_x^{'}\ t_y^{'}\ t_z^{'}\right]$ can be obtained and used in formula (7).

$$C_c^w = C_t^w C_b^t C_c^b \tag{8}$$

Error Equation of Dynamic Zero Velocity. In area D, the image features of two adjacent frames are used to judge whether the UAV is in a straight-line rollout state. when the UAV is in this state, the velocity error of the inertial sensor is restrained by the motion constraint of zero lateral velocity and vertical velocity. The specific methods are as follows:

The output velocity of the inertial sensor is v^t, the attitude conversion matrix is C_t^b, and the attitude conversion matrix between the UAV and the inertial sensor is C_b^m. Then,

$$\boldsymbol{v^m = C_b^m C_t^b v^t},\ \boldsymbol{v^{m'} = C_b^{m'} C_{t'}^b v^{t'}} \tag{9}$$

where $v^{t^{'}} = v^t + \delta v^t$, $v^{m^{'}} = v^m + \delta v^m$, $C_b^{m^{'}} = C_m^{m^{'}} C_b^m = (I - \delta\alpha\times)C_b^m$, $C_{t^{'}}^b = C_n^b C_{t^{'}}^n = C_t^b(I + \phi^t\times)$. Then,

$$\boldsymbol{\delta v^m = v^{m^{'}} - v^m = C_b^m(C_t^b \phi^t \times v^t + C_t^b \delta v^t) - \delta\alpha \times C_b^m C_t^b v^t} \tag{10}$$

where $\delta\alpha = \left[0\ \delta\alpha_\theta\ \delta\alpha_\psi\right]^T$.

Observation Equation. Based on the above analysis, the observation equation of the system is established as follows

$$\boldsymbol{Z = \left[K_B \cdot \delta L\ K_B \cdot \delta\lambda\ K_B \cdot \delta h\ K_D \cdot \delta v_x^m\ K_D \cdot \delta v_y^m\right]^T} \tag{11}$$

where

$$K_B = \begin{cases} 1 \text{ located in B or C} \\ 0 \text{ others} \end{cases}, K_D = \begin{cases} 1 \text{ located in D} \\ 0 \text{ others} \end{cases} \tag{12}$$

6 Experiment Verification

6.1 Experiment Conditions

The method proposed in this paper is verified by the actual flight data of a certain UAV, the flight experiment conditions are as follows:

1. The vision sensor is installed in a forward direction, the resolution of the vision sensor is 1024 × 768, and the horizontal field angle is 19.2°.
2. The performance of the inertial sensor is: the gyro bias stability is 0.5°/h; the accelerometer bias stability is 100 μg.
3. During landing, the UAV's track inclination is 2.5°. K1 = −200 m, K2 = −400 m, K3 = 750 m, K4 = 1500 m. The width of the runway is 50 m.
4. During the landing process, the satellite difference positioning data are collected synchronously, which is used as the reference to evaluate the method in this paper.

The lateral position error of runway coordinate system and visual sensor coordinate system plays a decisive role in landing safety, which is the most concerned relative position component in landing control. Generally, the lateral error cannot larger than 15 m. In order to evaluate the effectiveness of this method, the lateral errors of each region in the process of UAV landing are compared, and the performance curve of this method in the whole process of UAV landing is given.

6.2 Experiment Results

1. Location error analysis of area B. The UAV's flight duration in area B is about 15 s and the flight distance is about 800 m. The pure inertial lateral error diverges to 1.50 m and the visual measurement gives a lateral error of 0.30 m, as shown in Fig. 7(a).
2. Analysis of positioning error in area C. The UAV has a continuous flight time of 30 s in area C and a flight distance of about 1150 m. The traditional method uses inertial measurement to obtain the landing navigation parameters, and the lateral position error increases rapidly to 15.76 m, exceeding the allowable range (15 m). Using the method of inertial/visual information fusion given in this paper, the error of lateral position is within 1m in the first half. Because the error of the inertial measurement is corrected by visual measurement in the first half, it can still be controlled within 3.04 m at the end of the second half, as shown in Fig. 7(b).
3. Error analysis of area D positioning. The UAV has a continuous flight time of 40 s in area D and a sliding distance of 750 m. Traditional landing visual navigation methods cannot obtain landing navigation parameters at this stage and the lateral position error generated by inertial measurement increases rapidly from 3.04 m to 51.02 m. While the maximum lateral position error is 8.24 m using the inertial/visual information fusion method given in this paper, as shown in Fig. 7(c).
4. Analysis of comprehensive positioning error in the whole landing process of UAV. Figure 7(d) shows the comparison of lateral position error curves of different landing navigation strategies during the whole landing process of UAV. The cumulative lateral

error of the traditional landing visual navigation method is 68.47 m when the UAV stops, which does not meet the requirements of safe landing. The lateral error of proposed method is 8.24 m when the UAV stops, which reduces to 12% of the traditional method, meeting the requirements of safe landing.

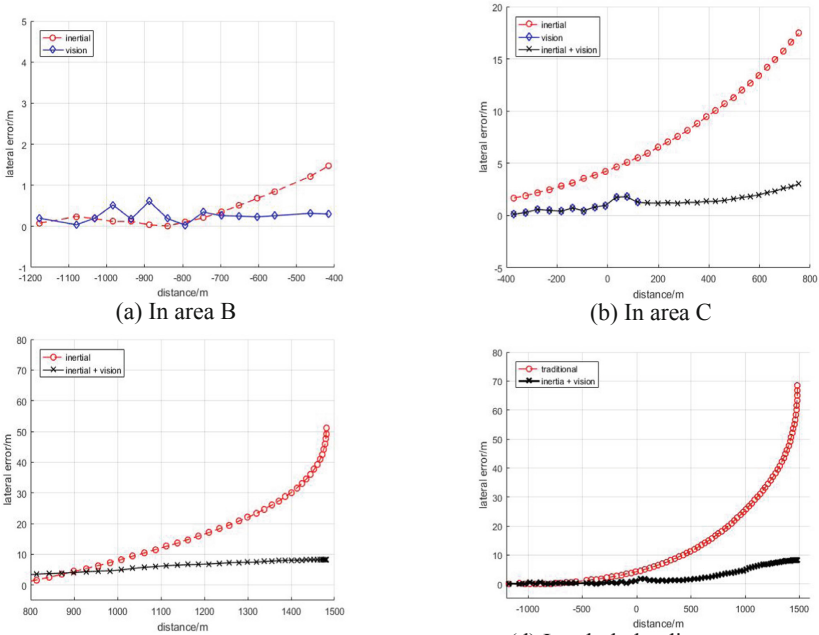

(a) In area B (b) In area C

(c) In area D (d) In whole landing progress

Fig. 7. Comparison of lateral errors

7 Conclusion

The vision sensor is affected by many factors during the landing process of UAV. Aiming at the instability of landing navigation parameters such as the relative position/attitude between UAV and runway, a method of autonomous landing navigation of UAV based on information fusion of inertial/vision sensor is proposed. The flight experiment shows that the lateral relative position error can reach 8.24 m under the condition of using low precision inertial and visual sensors, which can meet the requirement of UAV's safe landing. This paper provides a new low-cost strategy, fully autonomous solution for UAV landing, especially in complex electromagnetic environment.

References

1. Eitner, C., Holzapfel, F.: Development of a navigation solution for an image aided automatic landing system. In: Proceedings of the ION 2013 Pacific PNT Meeting, Honolulu, Hawaii, pp. 879–891, April 2013
2. Cai, M., et al.: Vision/INS integrated navigation for UAV autonomous landing. J. Appl. Opt. **36**(3), 343–350 (2015)
3. Wang, G., et al.: UAV autonomous landing using visual servo control based on aerostack. In: CSAE 2019, Sanya, China, October 2019
4. Zhou, H., et al.: Vision-based precision localization of UAVs for sensor payload placement and pickup for field monitoring applications. In: Proceedings Volume 10970, Sensors and Smart Structures Technologies for Civil, Mechanical, and Aerospace Systems 2019 (2019)
5. Wang, J., et al.: Integration of GPS/INS/vision sensors to navigate unmanned aerial vehicles. Int. Arch. Photogramm. Remote Sens. Spatial Inf. Sci. **37**, 963–969 (2008)
6. Zhang, L., et al.: Visual–inertial fusion-based registration between real and synthetic images in airborne combined vision system. Int. J. Adv. Robot. Syst. 1–14 (2019)
7. Wolkow, S., Angermann, M., Dekiert, A., Bestmann, U.: Model-based threshold and center-line detection for aircraft positioning during landing approach. In: Proceedings of the ION 2019 Pacific PNT Meeting, Honolulu, Hawaii, May 2019
8. Angermann, M., Wolkow, S., Dekiert, A., Bestmann, U., Hecker, P.: Fusion of dual optical position solutions for augmentation of GNSS-based aircraft landing systems. In: Proceedings of the 2019 International Technical Meeting of The Institute of Navigation, Reston, Virginia, pp. 283–295, January 2019
9. Angermann, M., Wolkow, S., Dekiert, A., Bestmann, U., Hecker, P.: Linear blend: data fusion in the image domain for image-based aircraft position during landing approach. In: Proceedings of the ION 2019 Pacific PNT Meeting, Honolulu, Hawaii, May 2019
10. Hesch, J.A., Roumeliotis, S.I.: A direct least-squares (DLS) method for PnP. In: Proceedings of 13th International Conference on Computer Vision. Barcelona, pp. 383–390 (2011)
11. Penate-Sanchez, A., Andrade-Cetto, J., Moreno-Noguer, F.: Exhaustive linearization for robust camera pose and focal length estimation. IEEE Trans. Pattern Anal. Mach. Intell. **35**(10), 2387–2400 (2013)
12. Ke-jun, S., Xin, Z., Wang Liu-jun, H., Guang-feng, L.-L.: Image semantic segmentation-based navigation method for UAV auto-landing. J. Chin. Inertial Technol. **28**(5), 1–9 (2020)
13. Li, F., Tang, D.-Q., Shen, N.: Vision-based pose estimation of UAV from line correspondences. Procedia Eng. **15**, 578–584 (2011)
14. Zhuang, L., Han, Y., Fan, Y., Cao, Y., Wang, B., Zhang, Q.: Method of pose estimation for UAV landing. Chin. Opt. Lett **10**(s2), S20401 (2012)
15. Wolkow, S., Schwithal, A., Tonhäuser, C., Angermann, M., Hecker, P.: Image-aided position estimation based on line correspondences during automatic landing approach. In: Proceedings of the ION 2015 Pacific PNT Meeting, Honolulu, Hawaii, pp. 702–712, April 2015
16. Dosse, M.B., Kiers, H.A.L., Ten Berge, J.: Anisotropic generalized procrustes analysis. Comput. Stat. Data Anal. **55**(5):1961–1968 (2011)
17. Garro, V., Crosilla, F., Fusiello, A.: Solving the pnp problem with anisotropic orthogonal procrustes analysis. In: 2012 Second Joint 3DIM/3DPVT Conference, Zurich, pp. 262–269 (2012)
18. Cai, Y., Li, D.: AUV underwater positioning method based on monocular-vision. J. Chin. Inertial Technol. **23**(4), 489–492 (2015)
19. Zhang, H., Guo, P., Li, Z.: Vision aided alignment method for inertial navigation system on moving base. J. Chin. Inertial Technol. **22**(4), 469–473 (2014)

20. Sun, T., Xing, F., You, Z.: Accuracy measurement of star trackers based on astronomy. J Tsinghua Univ. (Sci. Tech.) **52**(4), 430–435 (2012)
21. Liu, C., Liu, L., Hu, G., et al.: A P3P problem solving algorithm for landing vision navigation. Navig. Position. Timing **5**(1), 58–61 (2018)
22. Liu, C., Yang, L., Liu, F., et al.: Navigation algorithm based on inertial/vision information fusion of UAV autonomous landing. Navig. Position. Timing **3**(6), 6–11 (2016)
23. Schwithal, A., et al.: Integrity monitoring in GNSS/INS systems by optical augmentation. In: Inertial Sensors and Systems 2017, Karlsruhe, Germany (2017)
24. Angermann, M., Wolkow, S., Schwithal, A., Tonhäuser, C., Hecker, P.: High precision approaches enabled by an optical-based navigation system. In: Proceedings of the ION 2015 Pacific PNT Meeting, Honolulu, Hawaii, pp. 694–701, April 2015
25. Kim, S.B., Bazin, J.C., Lee, H.K., et al.: Ground vehicle navigation in harsh urban conditions by integrating inertial navigation system, global positioning system, odometer and vision data. Radar Sonar Navig. **5**(8), 814–823 (2011)
26. Georgy, J., Noureldin, A., Korenberg, M.J., et al.: Modeling the stochastic drift of a MEMS-based gyroscope in gyro/odometer/GPS integrated navigation. IEEE Trans. Intell. Transp. Syst. **11**(4), 856–872 (2010)
27. Dissanayake, G., Sukkarieh, S., Nebot, E., et al.: The aiding of a low-cost strapdown inertial measurement unit using vehicle model constraints for land vehicle applications. IEEE Trans. Robot. Autom. **17**(5), 731–747 (2001)
28. Gong, J., Liang, J., Wang, Y., et al.: On-line calibration method of SINS/DVL integrated navigation system. In: 2018 25th Saint Petersburg International Conference on Integrated Navigation Systems (ICINS)
29. Guo, F., Xie, L., Chen, J., et al.: Research of SINS/DVL/OD integrated navigation system based on observability analysis. In: 2016 35th Chinese Control Conference (CCC)
30. Jiang, Y., Lin, Y.: Error estimation of INS ground alignment through observability analysis. IEEE Trans. Aerosp. Electron. Syst. **28**(1), 92–96 (1992)